Structural Engineering and Mechanics, *Vol. 71, No. 6 (2019) 627-641*
DOI: https://doi.org/10.12989/sem.2019.71.6.627

Bending analysis of functionally graded plates with arbitrary shapes and boundary conditions

Monchai Panyatong*[1], Boonme Chinnaboon[2] and Somchai Chucheepsakul[2]

[1]*Department of Civil and Environmental Engineering, Faculty of Engineering, Rajamangala University of Technology Lanna, Chiang Rai, 57120, Thailand*
[2]*Department of Civil Engineering, Faculty of Engineering, King Mongkut's University of Technology Thonburi, Bangkok, 10140, Thailand*

(Received January 15, 2019, Revised April 14, 2019, Accepted April 18, 2019)

Abstract. The paper focuses on bending analysis of the functionally graded (FG) plates with arbitrary shapes and boundary conditions. The material property of FG plates is modelled by using the power law distribution. Based on the first order shear deformation plate theory (FSDT), the governing equations as well as boundary conditions are formulated and obtained by using the principle of virtual work. The coupled Boundary Element-Radial Basis Function (BE-RBF) method is established to solve the complex FG plates. The proposed methodology is developed by applying the concept of the analog equation method (AEM). According to the AEM, the original governing differential equations are replaced by three Poisson equations with fictitious sources under the same boundary conditions. Then, the fictitious sources are established by the application of a technique based on the boundary element method and approximated by using the radial basis functions. The solution of the actual problem is attained from the known integral representations of the potential problem. Therefore, the kernels of the boundary integral equations are conveniently evaluated and readily determined, so that the complex FG plates can be easily computed. The reliability of the proposed method is evaluated by comparing the present results with those from analytical solutions. The effects of the power index, the length to thickness ratio and the modulus ratio on the bending responses are investigated. Finally, many interesting features and results obtained from the analysis of the FG plates with arbitrary shapes and boundary conditions are demonstrated.

Keywords: functionally graded plate; boundary element method; analog equation method

1. Introduction

Functionally graded (FG) plates have been wildly exploited in many areas of engineering applications such as space plane bodies, solar panels, armor plates, an inner wall of nuclear reactors and fire-retardant doors due to their high thermal resistant and great strength. The FG plates are composite structures that have a continuous variation of material properties from one surface to another surface through the plate thickness, and thus eliminate the stress concentration which can be found in the laminate and sandwich plates. The variation of material properties may be modelled by the power law, sigmoid or exponential distributions. From the past researches, the high order shear deformation plate theories (HSDT) were used to evaluate the mechanical responses of FG plates. These models can capture the transverse shear deformation effect which is significant on mechanical responses of thick plates. For examples, Reddy (2000) formulated the governing equation of FG plates based on the third order shear deformation plate theory, and the solution was obtained by using Navier's solution and the finite element method. Qian *et al*. (2004) investigated the static and dynamic responses of FG plates by using the higher order shear and normal deformable plate theory (HOSNDPT), and the solutions were attained by the meshless local Petrov-Galerkin (MLPG) method. Najafizadeh and Heydari (2004) used the third order plate theory to investigate the thermal buckling of FG circular plates under thermal loads. Ferreira *et al*. (2006) employed the meshless method to compute the natural frequencies of FG plates of which material properties were homogenized by the Mori-Tanaka technique. Roque *et al*. (2007) analyzed the free vibration of FG plates by using a higher order shear deformation theory. The natural frequencies were solved by the multi-quadric radial basis function method. Shen (2007) studied thermal postbuckling of FG plates with temperature-dependent properties. The governing equations were developed by using a higher-order shear deformation plate theory. Talha and Singh (2010) studied the free vibration and static responses of FG plates, and the problems were solved by the finite element method. Wu and Li (2010) developed the Reissner mixed variational theorem based on a third-order shear deformation theory to study the static behavior of multilayered FG plates. The solution of simply supported FG plates was solved by double Fourier series. Reddy and Kim (2012) established the governing equation of FG plates based on a modified couple stress theory, the power law variation of the material through the plate thickness and the von Kármán nonlinear strains. Neves *et*

*Corresponding author, Ph.D.
E-mail: monchai_art@rmutl.ac.th

ISSN: 1225-4568 (Print), 1598-6217 (Online)

al. (2012) used the hyperbolic sine shear deformation theory to study the bending and free vibration of FG plates, and the radial basis function method was employed to obtain the solution. Recently, Daouadji and Adim (2017) presented a hyperbolic and parabolic shear and normal deformation theory for the bending analysis to account for the effect of thickness stretching in functionally graded sandwich plates. Aghazadeh *et al*. (2018) developed strain gradient elasticity-based procedures for static bending, free vibration and buckling analyses of functionally graded rectangular micro-plates. The effect of the length scale parameter on mechanical responses was studied. Bouhadra *et al*. (2018) proposed an improved higher shear deformation theory (HSDT) to consider the influence of thickness stretching in functionally graded (FG) plates. Analytical solutions of simply supported FG plates were presented.

Although the HSDT can accurately predict the behavior of FG plates, it may encounter many unknown variables in the problem, for examples, nine unknowns (Neves *et al*. 2012), eleven unknowns (Reddy and Kim 2012) and thirteen unknowns (Talha and Singh 2010). Thus, the advanced knowledge of mathematics is required to obtain the solution. Alternatively, the first order shear deformation plate theory (FSDT) is simple and has only three unknown variables (the in-plane displacements of the middle plane are neglected because it has a negligible effect for the small deflection problem). According to the FSDT, the transverse shear deformation is assumed to be constant with respect to the plate thickness. Therefore, the shear correction factor is required to match the actual parabolic distribution of the shear stresses through the plate thickness. The accurate results can be obtained by setting the appropriate shear correction factor. The FSDT was successfully applied to study the variety of the FG plate problems. For examples, Efraim and Eisenberger (2007) analyzed the free vibration of annular FG plates with variable plate thickness. The governing equation was developed by the FSDT, and the solution was obtained by using the exact element method and the dynamic stiffness method. Nguyen *et al*. (2008) examined the bending behavior of the sandwich panel with the functionally graded faces based on the FSDT. Hashemi *et al*. (2010) studied the free vibration of FG plates resting on the elastic foundations, and the analytical solution was developed to obtain the natural frequencies. Alshorbagy *et al*. (2013) developed the finite element method to investigate the thermo-mechanical response of FG plates. Ardestani *et al*. (2014) analyzed functionally graded stiffened plates by using the reproducing kernel particle method. The rectangular and circular FG plates were studied. Zhang and Liew (2016) analyzed the large deflection of quadrilateral FG plates with internal column supports. The element free IMLS-Ritz method was employed to derive the formulation of a discrete governing equation. Recently, Abad and Rouzegar (2017) investigated the free vibration of smart FG plates with integrated with piezoelectric layers. Amir *et al*. (2018) examined the post-buckling and geometrically nonlinear behaviors of moderately thick perfect and imperfect rectangular plates made-up of functionally graded materials. Spectral collocation approach based on Legendre basis functions was developed to analyze the functionally graded plates subjected to end-shortening strain.

In general, the FG plates are often confronted with the complexity of both geometries and boundary conditions. Unfortunately, the analytical solutions can be only determined from the simple cases. Thus, numerical solutions are required to solve the above issues. The finite element method (FEM) is an effective numerical technique for solving engineering problems. Nevertheless, it is ineffective and troublesome when the geometric bodies are comprised of holes or corners. The fine meshing and high-density elements are required at these critical domains and also take more time for computation. The boundary element method (BEM) is an alternative numerical method in which discretization is only performed over the boundary of the body, hence, reducing the number of the problem dimension by one order. However, the BEM can be only applied to the problems of which the fundamental solution can be established. For the plate problems having the coupled differential equations, the fundamental solutions are not obtainable; thus this method cannot be applied. To alleviate this restriction as mentioned above, Katsikadelis (2002) presented the analog equation method (AEM) that the original problem is converted to a substitute problem which so-called "*the analog equation*" under the fictitious sources with the same boundary and initial conditions. A simple equation with a known fundamental solution can be chosen as the analog equation. Then, the BEM is readily applied to solve the analog equation, and the solution of the original problem can be obtained from the integral representations of the substitute problem. At present, the AEM has been already successfully employed to solve the variety of engineering problems (Chinnaboon *et al*. 2007a, 2007b, 2011, Katsikadelis and Babouskos 2010, 2012, Yiotis and Katsikadelis 2013, Fam, *et al*. 2015, Babouskos and Katsikadelis 2015, Panyatong *et al*. 2018).

In this paper, a so-called coupled BE-RBF (Boundary Element-Radial Basis Function) method is developed to solve the FG plates with arbitrary shapes and boundary conditions. The governing equation of FG plates is formulated based on the first order shear deformation plate theory. The material properties in this study are varied through the plate thickness according to the power law distribution. The principle of virtual work is applied to establish the three differential governing equations as well as boundary conditions. The principle of the analog equation method is employed to develop the coupled BE-RBF method to solve the coupled differential equations. All advantages of the BEM are retained in this method that the discretization and integration are operated only on the boundary. The analog equations are composed of three Poisson equations which are linear equations having simple known fundamental solutions. The fictitious sources are approximated by the radial basis functions and established by using a BEM-based procedure. Hence, the solution of the original problem is conveniently established and easily evaluated. With the merits of the proposed methodology, this research fills a gap in the literature that the FG plates having arbitrary shapes (curve boundaries, corners,

openings, etc.) and boundary conditions can be investigated. The obtained results are compared with those from analytical solutions to verify the reliability of the present method. Then, the influences of the power index, the length to thickness ratio and the modulus ratio on the bending behavior are studied. Finally, the FG plate with arbitrary shapes and boundary conditions is analyzed to demonstrate the efficiency of the proposed method.

2. Theoretical problem

2.1 Material properties of FG plates

The functionally graded plates are highly heterogeneous material structures in which their properties vary through the plate thickness smoothly. In this study, the power law distribution is employed to describe the modulus of elasticity of the plate. While, the Poisson's ratio is defined to be constant because its effect is minimal on mechanical responses (Yang *et al*. 2005, Kitipornchai *et al*. 2006). According to the power law model, the modulus of elasticity of the FG plate through the plate thickness can be expressed as:

$$E(z) = E_m + (E_c - E_m)\left(\frac{h-2z}{2h}\right)^p \tag{1}$$

where E_c and E_m are the moduli of elasticity at the top surface (ceramic-rich) and the bottom surfaces (metal-rich) of the FG plate, respectively. Meanwhile, p is the power index of the material and h is the plate thickness. Moreover, the constitutive relationships of the FG plate can be represented by the following equation:

$$\begin{Bmatrix}\sigma_{xx}\\ \sigma_{yy}\\ \sigma_{xy}\\ \sigma_{xz}\\ \sigma_{yz}\end{Bmatrix} = \frac{E(z)}{1-\nu^2}\begin{bmatrix}1 & \nu & 0 & 0 & 0\\ \nu & 1 & 0 & 0 & 0\\ 0 & 0 & (1-\nu) & 0 & 0\\ 0 & 0 & 0 & (1-\nu) & 0\\ 0 & 0 & 0 & 0 & (1-\nu)\end{bmatrix}\begin{Bmatrix}\varepsilon_{xx}\\ \varepsilon_{yy}\\ \varepsilon_{xy}\\ \varepsilon_{xz}\\ \varepsilon_{yz}\end{Bmatrix} \tag{2}$$

where ν is Poisson's ratio.

2.2 The governing equations of FG plates

Consider a FG plate of a uniform thickness h, occupying the two-dimensional multiply connected domain Ω of the plane with the boundary $\Gamma \bigcup_{i=0}^{i=k} \Gamma_i$ as shown in Fig. 1. The curves (i = 0,1,2,…,K) may be piecewise smooth; that is the boundary may have a finite number of corners.

For the formulation in the present study, the first-order shear deformation plate theory is employed to derive the governing equations of FG plates. According to the FSDT, the displacement fields at any point depend only on the displacements of the middle plane of the FG plates which can be expressed as

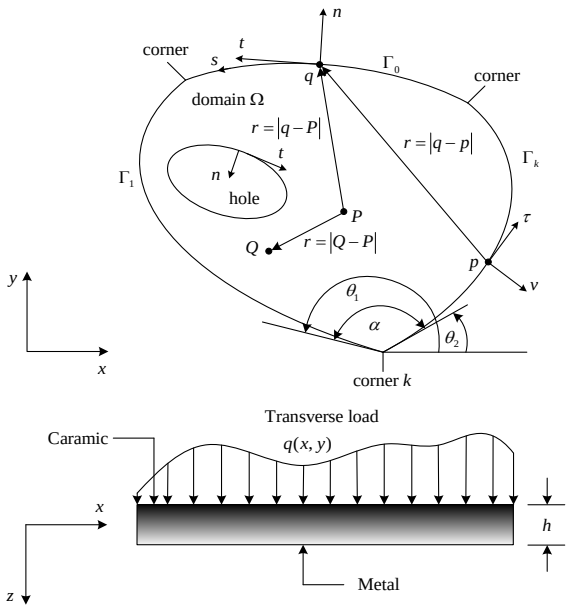

Fig. 1 A FG plate and notations

$$u = z\phi_x(x,y) \tag{3a}$$

$$v = z\phi_y(x,y) \tag{3b}$$

$$w = w(x,y) \tag{3c}$$

where u, v and w are the displacement components of any point in the directions x, y and z, respectively. Meanwhile, ϕ_x and $-\phi_y$ denote the rotations about the y and x-axes, respectively. For the sake of simplicity, the in-plane displacements of the middle surface are not taken into account in Eqs. (3a)-(3c). The work of Zhang and Zhou (2008) suggested that the in-plane displacements can be neglected in the small deflection problems. Also, the neutral surface in this study is assumed to coincide with the mid-surface of the plate, although the neutral surface of functionally graded plates may not coincide with its geometric mid-surface due to the material property variation through the plate thickness. The effect of considering and neglecting neutral plane positions has been investigated by Shaat *et al*. (2013) which reported a slight difference in central deflections and stress distributions.

By using the relations (3a)-(3c), the strains can be described by

$$\begin{Bmatrix}\varepsilon_{xx}\\ \varepsilon_{yy}\\ \varepsilon_{xy}\\ \varepsilon_{xz}\\ \varepsilon_{yz}\end{Bmatrix} = \begin{Bmatrix} z\phi_{x,x}\\ z\phi_{y,y}\\ z\left(\phi_{x,y}+\phi_{y,x}\right)\\ \frac{1}{2}\left(\phi_x + w_{,x}\right)\\ \frac{1}{2}\left(\phi_y + w_{,y}\right)\end{Bmatrix} \tag{4}$$

The governing equations of FG plates can be formulated by the application of the principle of virtual work as follows:

$$\delta U + \delta V = 0 \tag{5}$$

where δU and δV are the virtual strain energy and the virtual work done by applied loads, respectively. The virtual strain energy is given by

$$\delta U = \int_{\Omega}\int_{-h/2}^{h/2} \begin{pmatrix} \sigma_{xx}\delta\varepsilon_{xx} + \sigma_{yy}\delta\varepsilon_{yy} + 2\sigma_{xy}\delta\varepsilon_{xy} \\ +2\sigma_{xz}\delta\varepsilon_{xz} + 2\sigma_{yz}\delta\varepsilon_{yz} \end{pmatrix} dz\, d\Omega \tag{6}$$

and the virtual work done by the distributed load is provided by

$$\delta V = -\int_{\Omega} q\delta w\, d\Omega \tag{7}$$

Substituting Eq. (4) into Eq. (6) and using the constitutive relations (2), then, conducting the integration throughout the plate thickness and also using the Gauss-Green theorem, we obtain the governing equations as:

$$\delta w: \quad Q_{xz,x} + Q_{yz,y} + q = 0 \tag{8a}$$

$$\delta\phi_x: \quad -M_{xx,x} - M_{xy,y} + Q_{xz} = 0 \tag{8b}$$

$$\delta\phi_y: \quad -M_{yy,y} - M_{xy,x} + Q_{yz} = 0 \tag{8c}$$

with associated boundary conditions:

$$w = 0 \quad \text{or} \quad Q_{xz}n_x + Q_{yz}n_y = 0 \tag{9a}$$

$$\phi_x = 0 \quad \text{or} \quad M_{xx}n_x + M_{xy}n_y = 0 \tag{9b}$$

$$\phi_y = 0 \quad \text{or} \quad M_{yy}n_y + M_{xy}n_x = 0 \tag{9c}$$

where n_x and n_y are the components of the unit vector $\boldsymbol{n}$ which is normal to the boundary Γ (see Fig. 1). The bending moments and shear forces appearing in Eqs. (8a)-(8c) and the boundary conditions (9a)-(9c) can be provided by

$$M_{xx} = A\left(\phi_{x,x} + \nu\phi_{y,y}\right) \tag{10a}$$

$$M_{yy} = A\left(\phi_{y,y} + \nu\phi_{x,x}\right) \tag{10b}$$

$$M_{xy} = \frac{A}{2}(1-\nu)\left(\phi_{x,y} + \phi_{y,x}\right) \tag{10c}$$

$$Q_{xz} = k_s B\left(\phi_x + w_{,x}\right) \tag{10d}$$

$$Q_{yz} = k_s B\left(\phi_y + w_{,y}\right) \tag{10e}$$

where

$A = \dfrac{1}{(1-\nu^2)}\displaystyle\int_{-h/2}^{h/2} z^2 E(z)\, dz$ is the effective bending stiffness of the FG plate.

$B = \dfrac{1}{2(1+\nu)}\displaystyle\int_{-h/2}^{h/2} E(z)\, dz$ is the effective transverse shear stiffness of the FG plate and k_s is the shear correction factor. Finally, the governing equations of FG plates in terms of the deflection w and the rotations ϕ_x, ϕ_y can be obtained by substituting Eqs. (10a)-(10e) into Eqs. (8a)-(8c).

Therefore, we obtain the governing differential equations as:

$$-k_s B\left(\nabla^2 w + \phi_{x,x} + \phi_{y,y}\right) = q \tag{11a}$$

$$-\frac{A}{2}\left[(1-\nu)\nabla^2\phi_x + (1+\nu)\left(\phi_{x,xx} + \phi_{y,xy}\right)\right] + k_s B\left(\phi_x + w_{,x}\right) = 0 \tag{11b}$$

$$-\frac{A}{2}\left[(1-\nu)\nabla^2\phi_y + (1+\nu)\left(\phi_{x,xy} + \phi_{y,yy}\right)\right] + k_s B\left(\phi_y + w_{,y}\right) = 0 \tag{11c}$$

For convenience of programming, the boundary conditions, Eqs. (9a)-(9c), are rewritten in the following forms:

$$\alpha_1 w + \alpha_2 Q_n = \alpha_3 \tag{12a}$$

$$\beta_1\phi_n + \beta_2 M_n = \beta_3 \tag{12b}$$

$$\gamma_1\phi_t + \gamma_2 M_{nt} = \gamma_3 \tag{12c}$$

where Q_n, M_n and M_{nt} are the shear force resultant, bending moment and twisting moment along the boundary corresponding to the $n-t$ coordinates; ϕ_n and $-\phi_t$ are the rotations at the middle plane about the t and n axes, respectively (see Fig. 1). Meanwhile, $\alpha_i, \beta_i, \gamma_i \in \Gamma$ $(i = 1, 2, 3)$ are given functions specified on the boundary Γ. Evidently, all type of conventional boundary conditions can be obtained from Eqs. (12a)-(12c) by defining the functions α_i, β_i and γ_i appropriately as:

(a) clamped support if

$$\begin{aligned} &\alpha_1 = 1, \quad \alpha_2 = 0, \quad \alpha_3 = 0, \\ &\beta_1 = 1, \quad \beta_2 = 0, \quad \beta_3 = 0, \\ &\gamma_1 = 1, \quad \gamma_2 = 0, \quad \gamma_3 = 0. \end{aligned} \tag{13a}$$

(b) hard type simple support if

$$\begin{aligned} &\alpha_1 = 1, \quad \alpha_2 = 0, \quad \alpha_3 = 0, \\ &\beta_1 = 0, \quad \beta_2 = 1, \quad \beta_3 = 0, \\ &\gamma_1 = 1, \quad \gamma_2 = 0, \quad \gamma_3 = 0. \end{aligned} \tag{13b}$$

(c) soft type simple support if

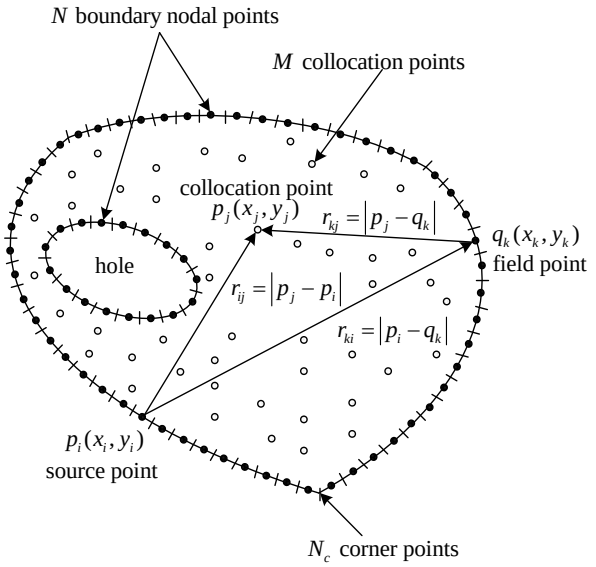

Fig. 2 Discretization of the FG plate

$$\begin{aligned} &\alpha_1 = 1, \quad \alpha_2 = 0, \quad \alpha_3 = 0, \\ &\beta_1 = 0, \quad \beta_2 = 1, \quad \beta_3 = 0, \\ &\gamma_1 = 0, \quad \gamma_2 = 1, \quad \gamma_3 = 0. \end{aligned} \tag{13c}$$

(d) free edge if

$$\begin{aligned} &\alpha_1 = 0, \quad \alpha_2 = 1, \quad \alpha_3 = 0, \\ &\beta_1 = 0, \quad \beta_2 = 1, \quad \beta_3 = 0, \\ &\gamma_1 = 0, \quad \gamma_2 = 1, \quad \gamma_3 = 0. \end{aligned} \tag{13d}$$

The shear force resultant, bending moment and twisting moment resultants on the boundary appearing Eqs. (12a)-(12c) can be written in term of the deflection w and the rotations ϕ_n, ϕ_t as follows:

$$Q_n = k_s B\left(\phi_n + w_{,n}\right) \tag{14a}$$

$$M_n = A\left(\phi_{n,n} + \nu\,\phi_{t,t}\right) \tag{14b}$$

$$M_{nt} = \frac{A}{2}(1-\nu)\left(\phi_{n,t} + \phi_{t,n}\right) \tag{14c}$$

Moreover, the relationships of the rotations between the $n-t$ coordinates and $x-y$ coordinates can be written as

$$\phi_n = n_x \phi_x + n_y \phi_y \tag{15a}$$

$$\phi_t = -n_y \phi_x + n_x \phi_y \tag{15b}$$

3. The coupled BE-RBF method for the FG plate

In this section, the coupled BE-RBF method is developed to solve the boundary value problem described by Eqs. (11a)-(11c) and (12a)-(12c). The present method will be developed based on the concept of the analog equation method (AEM) proposed by Katsikadelis (2002) that any differential equations can be replaced by other differential equations which have the same order under an unknown fictitious source. The substitute equations are called "*the analog equation*".

According to the AEM, the original governing equations of the FG plate are substituted by three Poisson equations with fictitious sources under the same boundary conditions. The solution of the actual problem can be attained from the known integral representations of Poisson equations. Therefore, the kernels of the boundary integral equations are conveniently determined and readily calculated. The procedure of the proposed method will be applied to the problem at hand as the following.

Let $w = w(x, y)$, $\phi_x = \phi_x(x, y)$ and $\phi_y = \phi_y(x, y)$ be the sought solutions of Eqs. (11a)-(11c). These functions are twice differentiable in the domain Ω and one time on its boundary Γ. By the application of the AEM, the differential operator that produces the substitute equations should be of the second order. The simplest operator of this order with known fundamental solutions is the Laplace operator. Thus, the substitute equations can be expressed as:

$$\nabla^2 w = b^{(1)}(x, y) \tag{16a}$$

$$\nabla^2 \phi_x = b^{(2)}(x, y) \tag{16b}$$

$$\nabla^2 \phi_y = b^{(3)}(x, y) \tag{16c}$$

Eqs. (16a)-(16c) are the analog equations of the FG plate problem and $b^{(l)}(x, y), l = 1, 2, 3$ are the three fictitious sources, unknown in the first instance. The solution of the analog equations can be achieved by using the BEM procedure. Thus, the solutions in integral forms can be expressed as:

$$\varepsilon w(p) = -\int_\Gamma \left(u^* w_{,n} - u^*_{,n} w\right) ds + \int_\Omega u^* b^{(1)} d\Omega \tag{17a}$$

$$\varepsilon \phi_x(p) = -\int_\Gamma \left(u^* \phi_{x,n} - u^*_{,n} \phi_x\right) ds + \int_\Omega u^* b^{(2)} d\Omega \tag{17b}$$

$$\varepsilon \phi_y(p) = -\int_\Gamma \left(u^* \phi_{y,n} - u^*_{,n} \phi_y\right) ds + \int_\Omega u^* b^{(3)} d\Omega \tag{17c}$$

where $u^* = (\ln r)/2\pi$ is the fundamental solution of the Laplace equation and $u^*_{,n} = r_{,n}/2\pi r$ is its normal derivative to the boundary at the field point q with $r = |p - q|$ (see Fig.1). Meanwhile, ε is the free term coefficient which is defined by

$$\varepsilon = \begin{cases} 1 & \text{for } p = P \text{ inside } \Omega, \\ \alpha / 2\pi & \text{for } p \text{ on the boundary } \Gamma, \\ 0 & \text{for } p \text{ outside } \Omega. \end{cases} \tag{18}$$

Eqs. (17a)-(17c) are the coupled domain and boundary integral equations, and it could be solved by using domain discretization to approximate the domain integrals. However, to maintain its pure boundary characteristic of the BEM, the domain integrals can be converted to the boundary integrals by approximating the fictitious sources with the radial basis functions (RBF). Thus, they can be written as:

$$b^{(l)} = \sum_{j=1}^{M} a_j^{(l)} f_j, \quad (l = 1,2,3) \tag{19}$$

where $f_j = f_j(r)$ is a set of radial basis approximating functions; $a_j^{(l)}$ are M coefficients (in a total of $3M$) to be determined and $r = |p_i - p_j|$ is the distance between the collocation point $p_j(x_j, y_j)$ and any point $p_i(x_i, y_i) \in \Omega \cup \Gamma$ (see Fig. 2). Then, using Green's second identity, the domain integrals in Eqs. (17a)-(17c) can be written as:

$$\int_{\Omega} u^* b^{(l)} d\Omega = \sum_{j=1}^{M} a_j^{(l)} \left\{ \varepsilon \hat{u}_j + \int_{\Gamma} \left(u^* \hat{u}_{j,n} - \hat{u}_j u_{,n}^* \right) ds \right\} \quad (l = 1,2,3) \tag{20}$$

where $\hat{u}_j = \hat{u}_j(r)$ is the particular solution of

$$\nabla^2 \hat{u}_j = f_j, \qquad j = 1,2,...,M. \tag{21}$$

The solution $\hat{u}_j = \hat{u}_j(r)$ of Eq. (21) can be always determined if f_j is specified. By substituting Eq. (20) into Eqs. (17a)-(17c), the solutions at a point $p \in \Gamma$ for smooth boundary can be expressed as:

$$\frac{1}{2} w(p) = -\int_{\Gamma} \left(u^* w_{,n} - u_{,n}^* w \right) ds + \sum_{j=1}^{M} a_j^{(1)} \left\{ \frac{1}{2} \hat{u}_j + \int_{\Gamma} \left(u^* \hat{u}_{j,n} - u_{,n}^* \hat{u}_j \right) ds \right\} \tag{22a}$$

$$\frac{1}{2} \phi_x(p) = -\int_{\Gamma} \left(u^* \phi_{x,n} - u_{,n}^* \phi_x \right) ds + \sum_{j=1}^{M} a_j^{(2)} \left\{ \frac{1}{2} \hat{u}_j + \int_{\Gamma} \left(u^* \hat{u}_{j,n} - u_{,n}^* \hat{u}_j \right) ds \right\} \tag{22b}$$

$$\frac{1}{2} \phi_y(p) = -\int_{\Gamma} \left(u^* \phi_{y,n} - u_{,n}^* \phi_y \right) ds + \sum_{j=1}^{M} a_j^{(3)} \left\{ \frac{1}{2} \hat{u}_j + \int_{\Gamma} \left(u^* \hat{u}_{j,n} - u_{,n}^* \hat{u}_j \right) ds \right\} \tag{22c}$$

The additional two integral equations are obtained from Eqs. (22b) and (22c) by first differentiating with respect to the tangential direction τ at the source point p (see Fig. 1). For the point p where the boundary is smooth, we obtain

$$\frac{1}{2} \phi_{x,\tau}(p) = -\int_{\Gamma} \left(u_{,\tau}^* \phi_{x,n} - u_{,n\tau}^* \left[\phi_x - \phi_x(p) \right] \right) ds + \sum_{j=1}^{M} a_j^{(2)} \left\{ \frac{1}{2} \hat{u}_{j,\tau} + \int_{\Gamma} \left(u_{,\tau}^* \hat{u}_{j,n} - u_{,n\tau}^* \left[\hat{u}_j - \hat{u}_j(p) \right] \right) ds \right\} \tag{23a}$$

$$\frac{1}{2} \phi_{y,\tau}(p) = -\int_{\Gamma} \left(u_{,\tau}^* \phi_{y,n} - u_{,n\tau}^* \left[\phi_y - \phi_y(p) \right] \right) ds + \sum_{j=1}^{M} a_j^{(3)} \left\{ \frac{1}{2} \hat{u}_{j,\tau} + \int_{\Gamma} \left(u_{,\tau}^* \hat{u}_{j,n} - u_{,n\tau}^* \left[\hat{u}_j - \hat{u}_j(p) \right] \right) ds \right\} \tag{23b}$$

Moreover, the derivatives of the deflection w and rotations ϕ_x, ϕ_y inside the domain Ω are obtained by direct differentiation of Eqs. (17a)-(17c). Thus, for the sake of conciseness, we can write the integral representations of the derivatives of the deflection w, rotations ϕ_x, ϕ_y and their derivatives up to second order as:

$$w_{,ab}(P) = -\int_{\Gamma} \left(u_{,ab}^* w_{,n} - u_{,nab}^* w \right) ds + \sum_{j=1}^{M} a_j^{(1)} \left\{ \hat{u}_{j,ab} + \int_{\Gamma} \left(u_{,ab}^* \hat{u}_{j,n} - u_{,nab}^* \hat{u}_j \right) ds \right\} \tag{24a}$$

$$\phi_{x,ab}(P) = -\int_{\Gamma} \left(u_{,ab}^* \phi_{x,n} - u_{,nab}^* \phi_x \right) ds + \sum_{j=1}^{M} a_j^{(2)} \left\{ \hat{u}_{j,ab} + \int_{\Gamma} \left(u_{,ab}^* \hat{u}_{j,n} - u_{,nab}^* \hat{u}_j \right) ds \right\} \tag{24b}$$

$$\phi_{y,ab}(P) = -\int_{\Gamma} \left(u_{,ab}^* \phi_{y,n} - u_{,nab}^* \phi_y \right) ds + \sum_{j=1}^{M} a_j^{(3)} \left\{ \hat{u}_{j,ab} + \int_{\Gamma} \left(u_{,ab}^* \hat{u}_{j,n} - u_{,nab}^* \hat{u}_j \right) ds \right\} \tag{24c}$$

where $a,b = 0,x,y$ and $P \in \Omega$. Note that $w_{,0} = w_{,00} = w$, $\phi_{x,0} = \phi_{x,00}$ and $\phi_{y,0} = \phi_{y,00} = \phi_y$.

Consider the governing equations described by Eqs. (11a)-(11c) and the boundary conditions (12a)-(12c), there are the total $8N$ variables on the boundary, i.e., w, $w_{,n}$, ϕ_x, $\phi_{x,n}$, $\phi_{x,t}$, ϕ_y, $\phi_{y,n}$ and $\phi_{y,t}$. We have $8N$ available equations comprised of: $5N$ boundary integral equations (22a)-(22c), (23a), (23b) and $3N$ equations from the prescribed boundary conditions (12a)-(12c). Therefore, we can solve this problem and obtain the $8N$ boundary quantities. In the next section, the implementation of the coupled BE-RBF method will be presented in details.

4. Numerical implementation

The boundary integrals in Eqs. (22a)-(22c) and (23a) and (23b) will be solved by the application of the BEM technique. The boundary elements may be constant, linear, or curves of higher order (e.g., quadratic, cubic). Nevertheless, employing the higher order must encounter the complicate numerical solution and the troublesome evaluation of singular integrals. On the other hand, using the constant elements can be conveniently evaluated for the singular integrals, and its numerical implementation is straightforward. Meanwhile, the accuracy can be improved by increasing the number of boundary elements. Therefore, in this study, the constant boundary element is employed to obtain the numerical solution of the boundary integral equations.

Let N and M be the numbers of the boundary nodal points and domain collocation points, respectively (see Fig. 2). Firstly, collocating at the N boundary nodes by using the boundary integrals (22a)-(22c), (23a) and (23b) and the boundary conditions (12a)-(12c) which give the total $8N$ equations. Therefore, we have the following system of the linear equations:

$$\mathbf{Ax} = \mathbf{Ca} \tag{25}$$

where $\mathbf{A}$ is the $8N \times 8N$ known matrix origination from the integrations of the kernels on the boundary elements and the known coefficients from the boundary conditions; $\mathbf{C}$ is the $8N \times 3M$ known coefficient matrix; $\mathbf{a} = [\mathrm{a}_j^{(1)}, \mathrm{a}_j^{(2)}, \mathrm{a}_j^{(3)}]^T$ is the $3M \times 1$ vector of the unknown variables. Meanwhile, $\mathbf{x} = [w, w_{,n}, \phi_x, \phi_{x,n}, \phi_{x,t}, \phi_y, \phi_{y,n}, \phi_{y,t}]^T$ is the $8N \times 1$ vector of the boundary quantities. Then, Eq. (25) is employed to express the vector $\mathbf{x}$ in terms of the unknown variable $\mathbf{a}$ as follows:

$$\mathbf{x} = \mathbf{A}^{-1}\mathbf{Ca} \tag{26}$$

Subsequently, collocating at the M collocation points inside domain Ω by employing the integrals equations (24a)-(24c) which are the values involving the deflection w and the rotations ϕ_x, ϕ_y and their derivatives. We have

$$\mathbf{W}_{,ab} = \mathbf{D}_{,ab}^{(1)}\mathbf{x}_1 + \mathbf{C}_{,ab}^{(1)}\mathbf{a}_j^{(1)} \tag{27a}$$

$$\boldsymbol{\phi}_{x,ab} = \mathbf{D}_{,ab}^{(2)}\mathbf{x}_2 + \mathbf{C}_{,ab}^{(2)}\mathbf{a}_j^{(2)} \tag{27b}$$

$$\boldsymbol{\phi}_{y,ab} = \mathbf{D}_{,ab}^{(3)}\mathbf{x}_3 + \mathbf{C}_{,ab}^{(3)}\mathbf{a}_j^{(3)} \tag{27c}$$

where $\mathbf{x}_1 = \left[w, w_{,n}\right]^T$, $\mathbf{x}_2 = \left[\phi_x, \phi_{x,n}\right]^T$ and $\mathbf{x}_3 = [\phi_y, \phi_{y,n}]^T$ are the $2N \times 1$ vectors of the boundary quantities which are the complements of the vector $\mathbf{x}$. By substituting the components of the vector $\mathbf{x}$ from Eq. (26) into Eqs. (27a)-(27c) appropriately, they can be expressed regarding unknown variable of the vector $\mathbf{a}$ as:

$$\mathbf{W}_{,ab} = \mathbf{H}_{,ab}^{(1)}\mathbf{a} \tag{28a}$$

$$\boldsymbol{\phi}_{x,ab} = \mathbf{H}_{,ab}^{(2)}\mathbf{a} \tag{28b}$$

$$\boldsymbol{\phi}_{y,ab} = \mathbf{H}_{,ab}^{(3)}\mathbf{a} \tag{28c}$$

Finally, by substituting Eqs. (28a)-(28c) into the governing equations (12a)-(12c), we obtain the following system of the $3M$ linear equations as:

$$\mathbf{Sa} = \mathbf{d} \tag{29}$$

Then, solving Eq. (29) yields the $3M$ unknown variables of the vector $\mathbf{a}$. Thereafter, the values of the deflection w and the rotations ϕ_x, ϕ_y and their derivatives inside the domain Ω can be obtained from Eqs. (24a)-(24c). Meanwhile, the resultant forces can be determined by using Eqs. (10a)-(10e). For the point P not coinciding with the collocation domain points, the respective quantities can be established from the discretized counterparts of Eqs. (24a)-(24c).

5. Numerical results and discussion

5.1 Reliability of the proposed method

In order to manifest the reliability of the proposed method, a computer program has been developed and used to analyze the simply supported square plate ($a \times a$) with isotropic and FG materials (Al/Al_2O_3). The material properties of Al and Al_2O_3 are given in Table 1, and the shear correction factor (k_s) is 5/6. The accuracy of the proposed technique is evaluated by comparing the obtained results with the analytical ones. The analytical results can be determined by Navier's approach which is given in detail in the Appendix.

In this study, the Thin Plate Splines (TPSs) is used as the radial basis approximation functions f_j, which was previously employed for analyzing plate problems (Chinnaboon *et al*. 2007a, Panyatong *et al*. 2018). The advantages of this function are that no shape parameters are required for obtaining the solution, and the derivatives of the particular solution $\hat{u}_j$ can be easily treated when the value of r approaching zero. The TPSs can be expressed as:

$$f_j = r^2 \ln r \tag{30}$$

The involved derivatives of $\hat{u}_j$ are also provided in the Appendix. The numerical results have been evaluated by using N = 200 constant boundary elements and M = 324 internal collocation points. The deflections and bending moments of the isotropic plate are contained in Table 2. Moreover, for the FG plate, the deflections with various power indexes are listed in Table 3. It is apparent that the present solutions are in very good accordance with the analytical results obtained by Navier's approach (see

Table 1 Mechanical properties of the FG plate

Materials		Modulus of Elasticity, (GPa)	Poisson's ratio
Metal	Aluminum (Al)	70	0.30
Ceramic	Alumina (Al_2O_3)	380	0.30

Table 2 The deflections and bending moments at the center of the simply supported (hard type) isotropic plate

h/a	Deflection, $\bar{w}=\frac{1000Dw}{qa^4}$		Bending moment, $\bar{M}_{xx}=\frac{100M_{xx}}{qa^2}$	
	Analytical	present	Analytical	present
0.05	4.1150	4.0626	4.7886	4.7406
0.10	4.2728	4.2514	4.7886	4.7666
0.15	4.5360	4.5239	4.7886	4.7719
0.20	4.9043	4.8992	4.7886	4.7738
0.25	5.3779	5.3801	4.7886	4.7746
0.30	5.9568	5.9671	4.7886	4.7751

Appendix A.1). Thus this comparison confirms the reliability of the proposed technique.

5.2 Parametric studies

In this section, the numerical results are presented to investigate the bending response of the square Al/Al_2O_3 plates $(a\times a)$ with various boundary conditions as shown in Fig. 3. All of the obtained results are computed by using N = 200 constant boundary elements and M = 324 internal collocation points. The effect of the power index on the central deflection of the FG plates with different h/a is illustrated in Figs. 4(a)-4(c). It is obviously seen that all figures show a similar trend, i.e., the increasing value of the power index produces a significant increase in the deflection for all boundary conditions. This is due to the fact that modulus of elasticity of the Al/Al_2O_3 plates approaches the modulus of elasticity of fully metal (Aluminum) when the power index is increasing. This phenomenon can be observed in Fig. 5 which displays the distribution of modulus of elasticity of the Al/Al_2O_3 plate through the plate thickness with various power indexes. It can be seen that the high value of the power index tends to converge the modulus of elasticity of the FG plate to the modulus of the fully metal.

The distributions of the normal stress σ_{xx} at the center of the Al/Al_2O_3 plate ($h/a=0.2$) corresponding to each case of boundary conditions are depicted in Figs. 6(a)-6(d). It can be seen that the maximum compressive stresses occur at the top surface for all power indexes and the high power indexes give more stress magnitudes than the low ones. Meanwhile, the position and magnitude of the maximum tensile stresses are varied that are controlled by the value of the power index. The magnitude of the tensile stresses is reduced when the power index increases. The tensile stresses at the bottom surface have close values for the

Table 3 The deflections at the center of the simply supported (hard type) Al/Al_2O_3 plate

h/a	Power index, p	$\bar{w}=\frac{100E_c h^3 w}{qa^4}$	
		Analytical	present
0.15	0.5	7.0749	7.0553
	1	8.3655	8.3433
	2	9.8230	9.8000
	5	12.2459	12.2223
	10	14.8993	14.8714
0.20	0.5	7.6274	7.6185
	1	9.0449	9.0355
	2	10.7049	10.6975
	5	13.5022	13.4995
	10	16.4561	16.4539
0.25	0.5	8.3378	8.3399
	1	9.9183	9.9223
	2	11.8387	11.8482
	5	15.1175	15.1381
	10	18.4578	18.4844

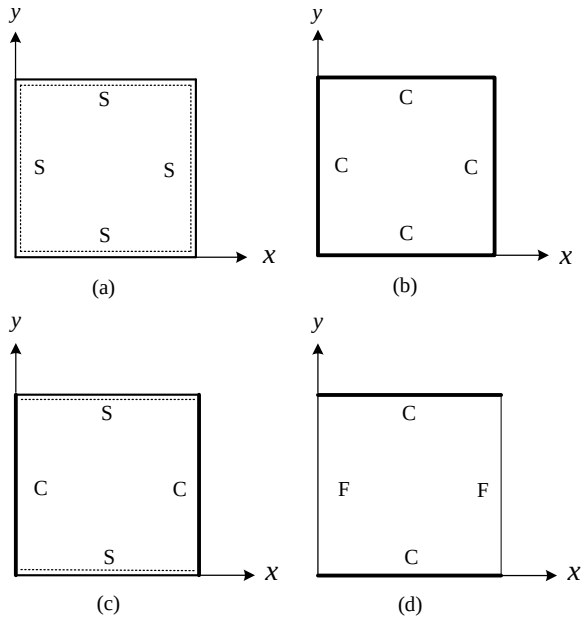

Fig. 3 Al/Al_2O_3 square plates with various boundary conditions, (S = Simple support, C = Clamped support, F = Free edge)

power indexes $p=0.5, 1, 2$, and they are smaller than the tensile stress of $p=0$ because the magnitudes of the moduli of elasticity $E(z)$ around the bottom region of $p=0.5, 1, 2$ are smaller than the $p=0$. It is worth noticing that the distribution of the normal stress is a linear relationship when the power index is zero, i.e., the fully ceramic homogeneous plate.

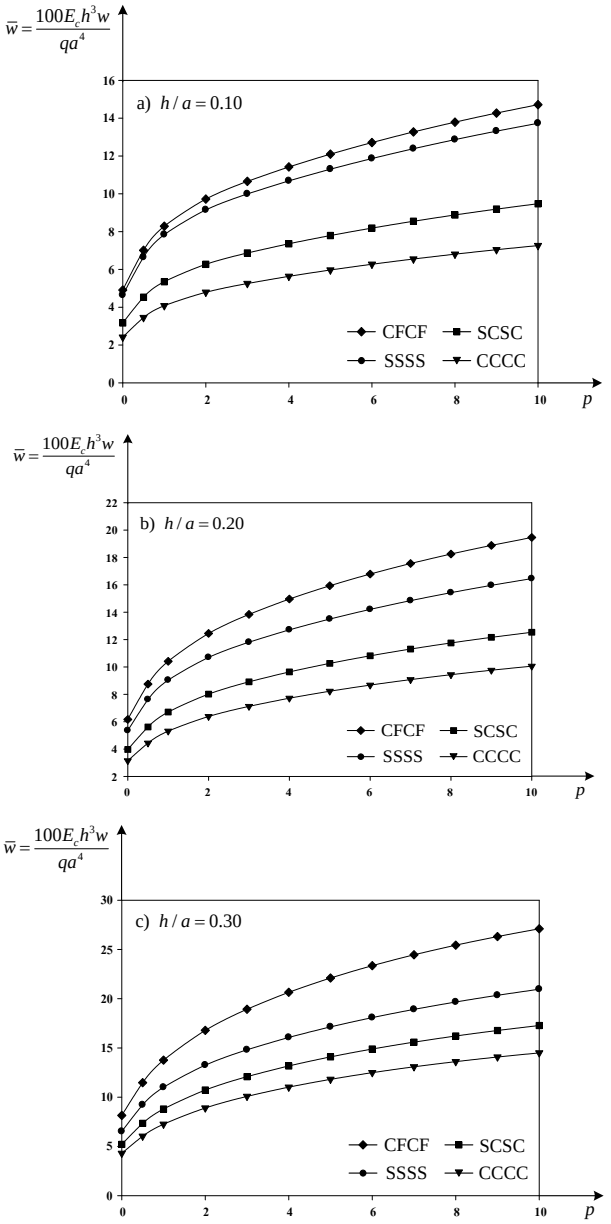

Fig. 4 The relationships between the central deflection and power index with different h/a

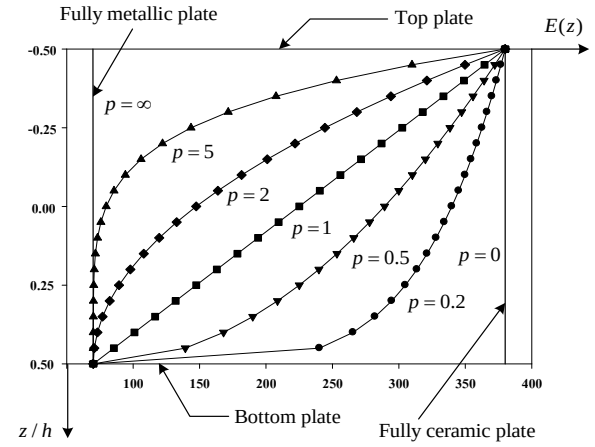

Fig. 5 The distribution of modulus of elasticity of the Al/Al_2O_3 plate through the plate thickness

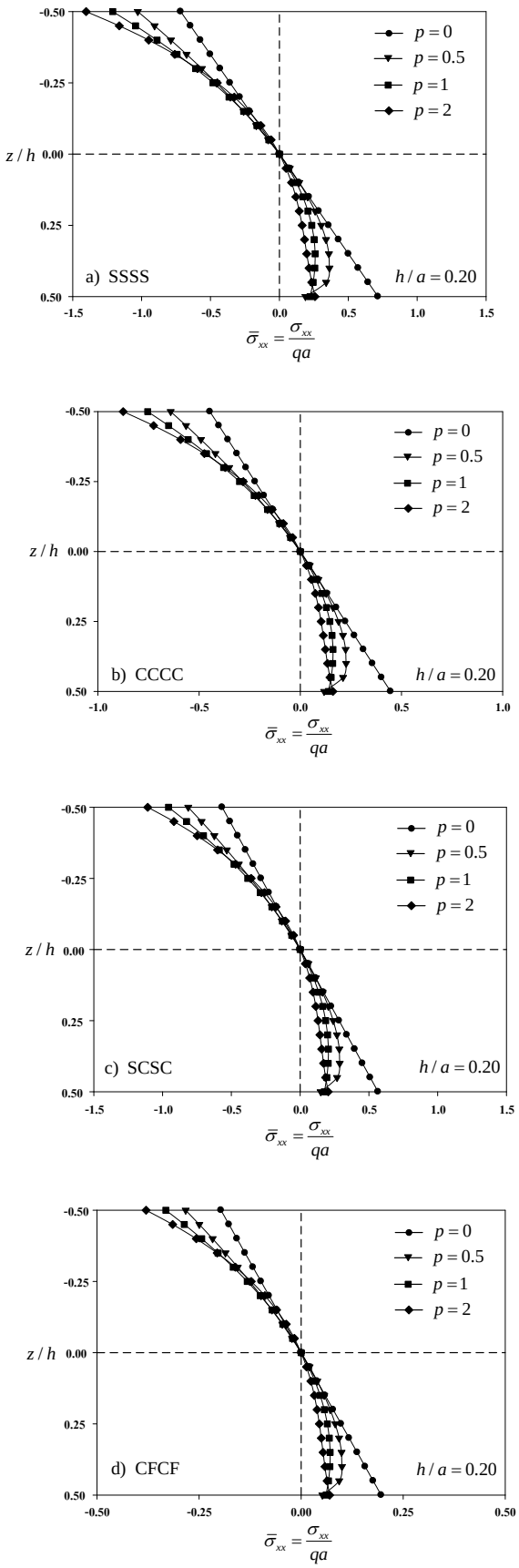

Fig. 6 The distributions of the normal stress σ_{xx} at the center of the Al/Al_2O_3 plate with various power indexes

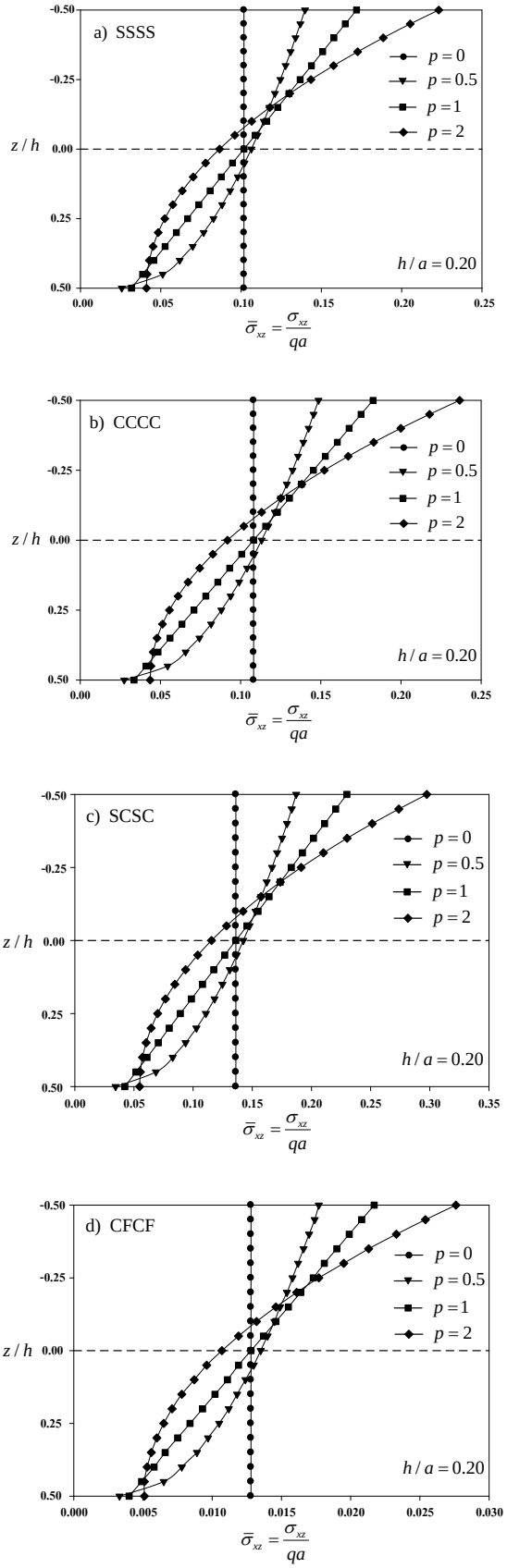

Fig. 7 The distributions of the shear stress σ_{xz} of the Al/Al_2O_3 plate with various power indexes at $x/a = 0.2$ and $y/a = 0.5$

Furthermore, the distributions of the shear stresses σ_{xz} through the plate thickness at $x/a = 0.2$ and $y/a = 0.5$ are displayed in Figs. 7(a)-7(d). According to the FSDT that the transverse shear deformation is assumed to be constant through the plate thickness, the obtained shear stresses appear at the top and bottom surfaces of the FG plate. Moreover, the distributions of the shear stresses depend on the value of the power index. The maximum shear stresses arise at the top surface and the high values of the power indexes provide more stress magnitudes than the low ones. However, the minimum shear stresses have the close magnitudes and occur at the bottom surface for the power indexes $p = 0.5, 1, 2$. For the homogeneous plate, the shear stresses are found to be constant through the plate thickness when $p = 0$.

The influences of the length to thickness ratio (a / h) on the central deflection $\bar{w}$ are displayed in Figs. 8(a)-8(d). It is apparent that an increase in the length to thickness ratio leads to a decrease in the central deflection $\bar{w}$ for all boundary conditions. Especially, for $a/h < 10$, there has been a rapid decrease in the central deflection $\bar{w}$ because the effect of shear deformation is diminished when the plate has a high length to thickness ratio. Moreover, the influence of the length to thickness ratio has very little domination over the central deflection $\bar{w}$ for $a/h > 10$. Also, it can be observed that the FG plates with the low power index possess more bending stiffness than those with the high power index.

Figs. 9(a)-9(d) shows the effect of the modulus ratio E_c / E_m on the central deflection $\bar{w}$ with various power indexes. They reveal that an increase in the modulus ratio leads to a gradual drop in the central deflection $\bar{w}$ for p = 0.5, 1 and 2. Meanwhile, the central deflection $\bar{w}$ rapidly decreases when p = 5 and remains steady when p = 0. This behavior can be explained that an increase in the modulus ratio enhances the bending stiffness of the FG plate. For the FG plate with p = 0, the modulus of elasticity of the FG plate through the plate thickness is homogeneous and equal to the modulus of elasticity of the fully ceramic E_c. Thus, the modulus ratio has no effect on the deflection for p = 0.

The highlight of this work is to develop the method which can solve the FG plates with the complexity of both geometries and boundary conditions. To demonstrate the abovementioned issue, the FG plate as shown in Fig. 10 has been analyzed. The FG plate has thickness h = 0.25 m, and it is subjected to a uniform load $q = 1\,\text{MPa}$. The numerical results have been obtained by using N = 1050 constant boundary elements and M = 204 internal collocation points. The material properties of Al and Al_2O_3 in Table 1 and $k_s = 5/6$ are used for this analysis. The variations of the computed deflections w and the bending moments M_{xx} along the x-axis at $y = 7.5\,\text{m}$ with the different power indexes are illustrated in Fig. 11. Hence, the proposed method can be regarded as an efficient numerical tool for analyzing FG plates with arbitrary shapes and boundary conditions.

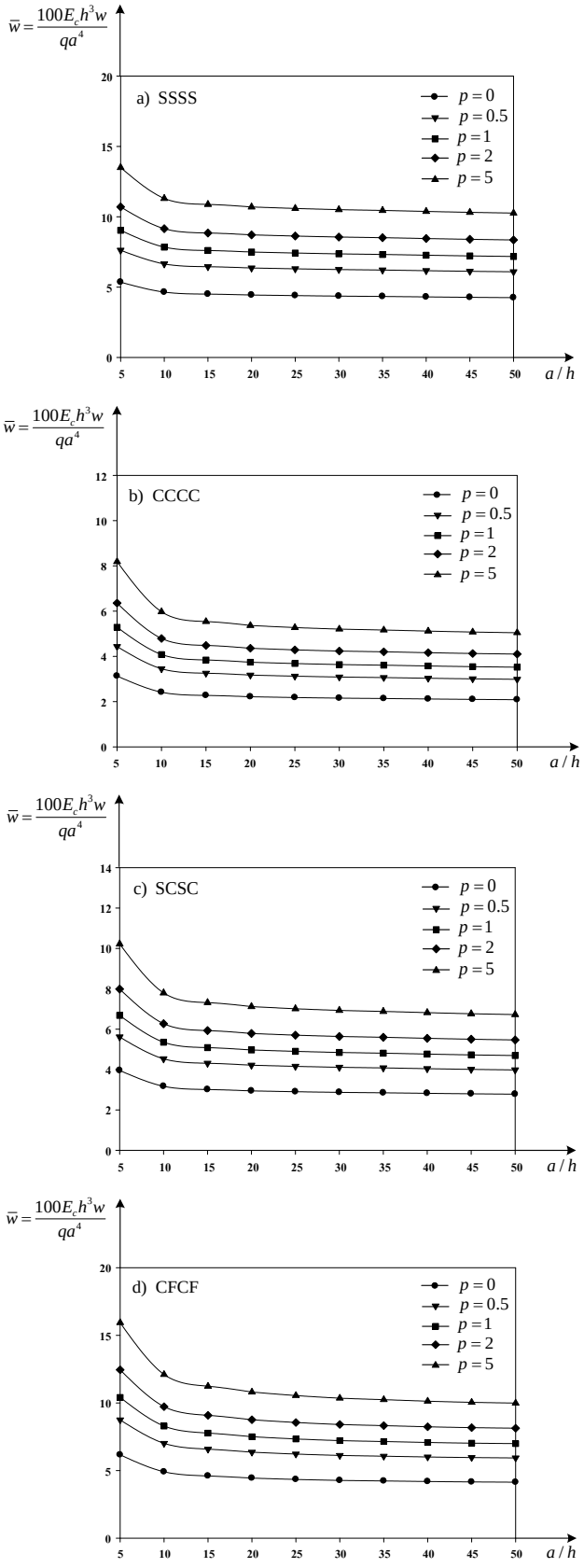

Fig. 8 The relationships between the length to thickness ratio and central deflection of the Al/Al_2O_3 plate with various power indexes

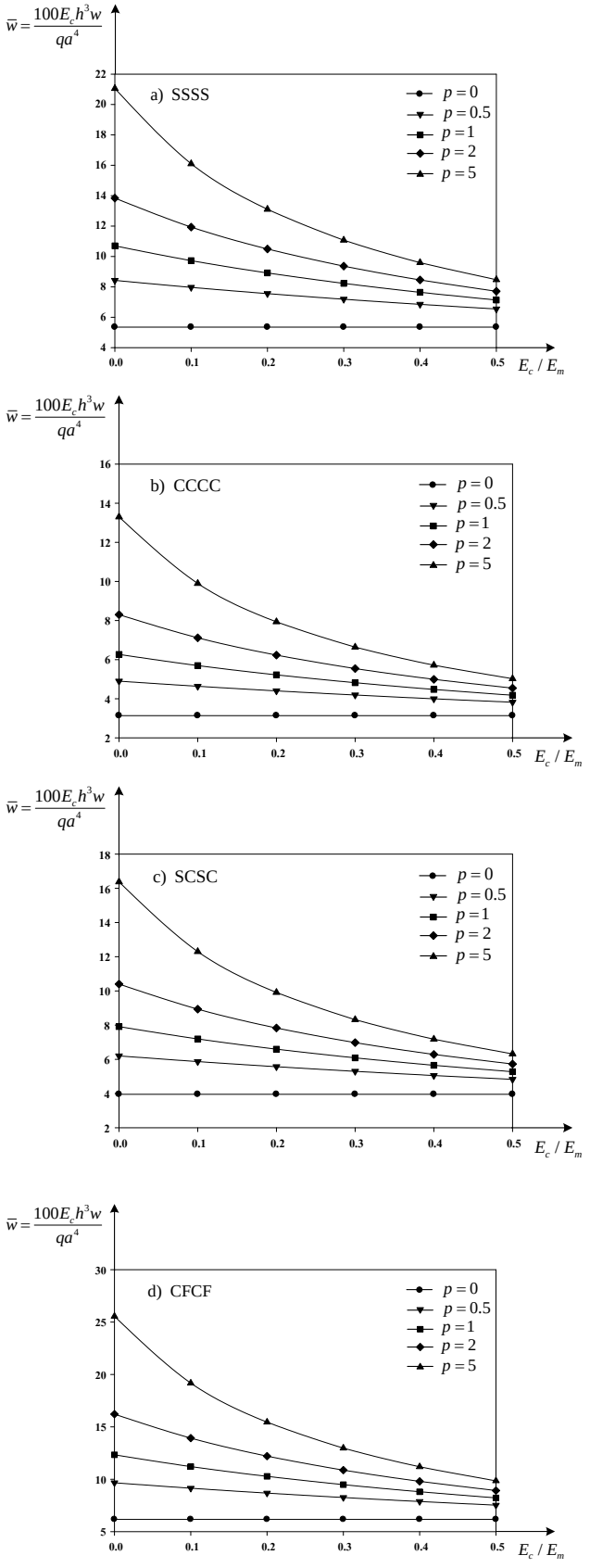

Fig. 9 The relationships between the modulus ratio and central deflection of the FG plate ($h/a=0.2$) with various power indexes

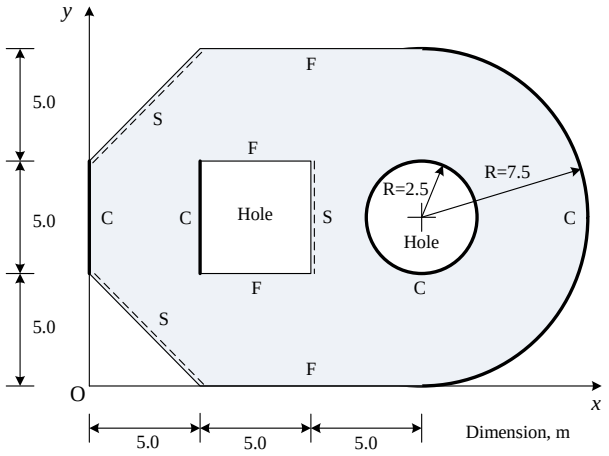

Fig. 10 The Al/Al_2O_3 plate with the complex shape and boundary condition

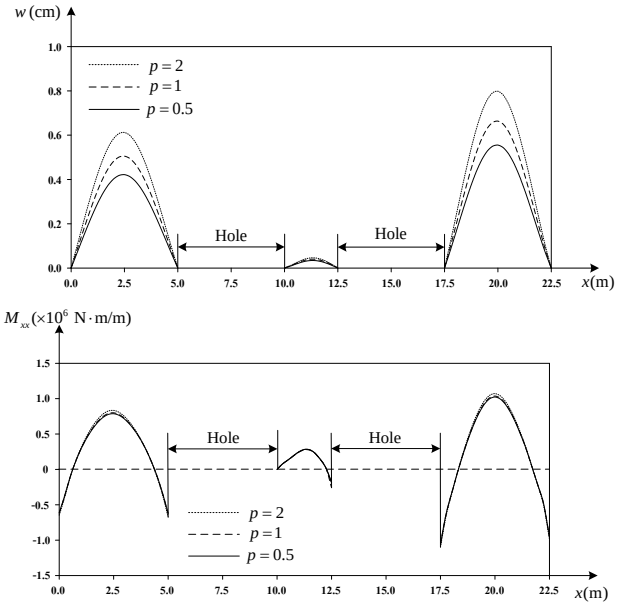

Fig. 11 The deflection and bending moment along the x-axis at $y = 7.5$ m

6. Conclusions

The governing equations of the FG plate are formulated based on the first-order shear deformation plate theory and the power law model for the material property distribution. The coupled BE-RBF method is established to solve the three differential governing equations of the FG plate. The present method is developed by applying the principle of the analog equation. The original governing differential equations are substituted by the three uncoupled Poisson equations with fictitious sources under the same boundary conditions. The fictitious sources are established by using a technique based on the BEM and approximated by using Thin Plate Splines (TPSs) as the radial basis functions. Consequently, the solution of the actual problem is attained from the known integral representations of the potential problem which are derived from the fundamental solution of the Laplace operator.

From the numerical results in this study, they are in excellent agreement with those from the analytical solutions, thus confirming the validity of the proposed method. Furthermore, the effects of the power index, the length to thickness ratio and the modulus ratio on the bending responses are investigated. Finally, the application of this methodology is demonstrated by solving the FG plate having the complex geometry and boundary condition. In this respect, the proposed methodology can be regarded as an efficient numerical tool for bending analysis of the FG plates with arbitrary shapes and boundary conditions.

Acknowledgments

The authors would like to acknowledge the Institutional Research Capability Development Grant from Thailand Research Fund (TRF) and King Mongkut's University of Technology Thonburi (KMUTT).

References

Abad, F. and Rouzegar, J. (2017), "An exact spectral element method for free vibration analysis of FG plate integrated with piezoelectric layers", *Compos. Struct.*, **180**, 696-708. https://doi.org/10.1016/j.compstruct.2017.08.030.

Aghazadeh, R., Dag, S. and Cigeroglu, E. (2018), "Modelling of graded rectangular micro-plates with variable length scale parameters", *Struct. Eng. Mech.,* **65**(5), 573-585. https://doi.org/10.12989/sem.2018.65.5.573.

Alshorbagy, A.E., Alieldin, S.S., Shaat, M. and Mahmoud, F.F. (2013), "Finite element analysis of the deformation of functionally graded plates under thermomechanical loads", *Math. Probl. Eng.*, **2013**. http://dx.doi.org/10.1155/2013/569781.

Amir, S., Ghannadpour, M., and Kiani, P. (2018), "Nonlinear spectral collocation analysis of imperfect functionally graded plates under end-shortening", *Struct. Eng. Mech.*, **66**(5), 557-568. https://doi.org/10.12989/sem.2018.66.5.557.

Ardestani, M.M., Soltani, B. and Shams, Sh. (2014), "Analysis of functionally graded stiffened plates based on FSDT utilizing reproducing kernel particle method", *Compos. Struct.*, **112**, 231-240. https://doi.org/10.1016/j.compstruct.2014.01.032.

Babouskos, N.G. and Katsikadelis, J.T. (2015), "Optimum design of thin plates via frequency optimization using BEM", *Arch. Appl. Mech.*, **85**(9-10), 1175-1190. https://doi.org/10.1007/s00419-014-0962-7.

Bouhadra A., Tounsi, A., Bousahla, A., Benyoucef, S. and Mahmoud, S.R. (2018), "Improved HSDT accounting for effect of thickness stretching in advanced composite plates", *Struct. Eng. Mech.*, **66**(1), 61-73.

Chinnaboon, B., Chucheepsakul, S. and Katsikadelis, J.T. (2007a), "A BEM-based meshless method for elastic buckling analysis of plates", *Int. J Struct. Stabil. Dynam.*, **7**(1), 81-99. https://doi.org/10.1142/S0219455407002162.

Chinnaboon, B., Chucheepsakul, S. and Katsikadelis, J.T. (2011), "A BEM-based domain meshless method for the analysis of Mindlin plates with general boundary conditions", *Comput. Meth. Appl. Mech. Eng.*, **200**(13-16), 1379-1388. https://doi.org/10.1016/j.cma.2010.12.014.

Chinnaboon, B., Katsikadelis, J.T. and Chucheepsakul, S. (2007b), "A BEM-based meshless method for plates on biparametric elastic foundation with internal supports", *Comput. Meth. Appl. Mech. Eng.*, **197**(33-34), 3165-3177. https://doi.org/10.1016/j.cma.2007.02.012.

Daouadji, T.H. and Adim, B. (2017), "Mechanical behavior of FGM sandwich plates using a quasi-3D higher order shear and normal deformation theory", *Struct. Eng. Mech.*, **61**(1), 49-63. https://doi.org/10.12989/sem.2017.61.1.049**.**

Efraim, E. and Eisenberger, M. (2007), "Exact vibration analysis of variable thickness thick annular isotropic and FGM plates", *J. Sound Vib.*, **299**(4-5), 720-738. https://doi.org/10.1016/j.jsv.2006.06.068.

Fam, G.S.A., Rashed, Y.F. and Katsikadelis, J.T. (2015), "The analog equation integral formulation for plane piezoelectric media", *Eng. Anal. Bound. Elem.*, **51**, 199-212. https://doi.org/10.1016/j.enganabound.2014.10.013.

Ferreira, A.J.M., Batra, R.C., Roque, C.M.C., Qian, L.F. and Jorge, R.M.N. (2006), "Natural frequencies of functionally graded plates by a meshless method", *Compos. Struct.*, **75**(1-4), 593-600. https://doi.org/10.1016/j.compstruct.2006.04.018.

Hashemi, S.H., Taher, H.R.D., Akhavan, H. and Omidi, M. (2010), "Free vibration of functionally graded rectangular plates using first-order shear deformation plate theory", *Appl. Math. Model.*, **34**(5), 1276-1291. https://doi.org/10.1016/j.apm.2009.08.008.

Katsikadelis, J.T. (2002), "The analog boundary integral equation method for nonlinear static and dynamic problem in continuum mechanics", *Int. J Theor. Appl. Mech.*, **40**(4), 961-984.

Katsikadelis, J.T. and Babouskos, N.G. (2010), "Post-buckling analysis of viscoelastic plates with fractional derivative models", *Eng. Anal. Bound. Elem.*, **34**(12), 1038-1048. https://doi.org/10.1016/j.enganabound.2010.07.003.

Katsikadelis, J.T. and Babouskos, N.G. (2012), "Stiffness and buckling optimization of thin plates with BEM", *Arch. Appl. Mech.*, **82**(10-11), 1403-1422. https://doi.org/10.1007/s00419-012-0668-7.

Kitipornchai, S., Yang, J. and Liew, K.M. (2006), "Random vibration of the functionally graded laminates in thermal environments", *Comp. Meth. Appl. Mech. Eng.*, **195**(9-12), 1075-1095. https://doi.org/10.1016/j.cma.2005.01.016.

Najafizadeh, M.M. and Heydari H.R. (2004), "Thermal buckling of functionally graded circular plates based on higher order shear deformation plate theory", *Eur. J Mech. Solid.*, **23**(6), 1085-1100. https://doi.org/10.1016/j.euromechsol.2004.08.004.

Neves, A.M.A., Ferreira, A.J.M., Carrera, E., Cinefra, M., Roque, C.M.C., Jorge, R.M.N. and Soares, C.M.M. (2012), "A quasi-3D hyperbolic shear deformation theory for the static and free vibration analysis of functionally graded plates", *Compos. Struct.*, **94**(5), 1814-1825. https://doi.org/10.1016/j.compstruct.2011.12.005.

Nguyen, T.K., Sab, K. and Bonnet, G. (2008), "First-order shear deformation plate models for functionally graded materials", *Compos. Struct.*, **83**, 25-36. https://doi.org/10.1016/j.compstruct.2007.03.004.

Panyatong, M., Chinnaboon, B. and Chucheepsakul, S. (2018), "Nonlinear bending analysis of nonlocal nanoplates with general shapes and boundary conditions by the boundary-only method", *Eng. Anal. Bound. Elem.*, **87**, 90-110. https://doi.org/10.1016/j.enganabound.2017.12.003.

Qian, L.F., Batra, R.C. and Chen, L.M. (2004), "Static and dynamic deformations of thick functionally graded elastic plates by using higher-order shear and normal deformable plate theory and meshless local Petrov-Galerkin method", *Compos. B Eng.*, **35**(6-8), 685-697. https://doi.org/10.1016/j.compositesb.2004.02.004.

Reddy, J.N. (2000), "Analysis of functionally graded plates", *Int. J. Numer. Meth. Eng.*, **47**(1-3), 663-684. https://doi.org/10.1002/(SICI)1097-0207(20000110/30)47:1/3%3C663::AID-NME787%3E3.0.CO;2-8

Reddy, J.N. and Kim, J. (2012), "A nonlinear modified couple stress-based third-order theory of functionally graded plates", *Compos. Struct.*, **94**(3), 1128-1143. https://doi.org/10.1016/j.compstruct.2011.10.006.

Roque, C.M.C., Ferreira, A.J.M. and Jorge, R.M.N. (2007), "A radial basis function approach for the free vibration analysis of functionally graded plates using a refined theory", *J. Sound Vib.*, **300**(3-5), 1048-1070. https://doi.org/10.1016/j.jsv.2006.08.037.

Shaat, M., Mahmoud, F.F., Alshorbagy, A.E. and Alieldin, S.S. (2013), "Bending analysis of ultra-thin functionally graded Mindlin plates incorporating surface energy effects", *Int. J Mech. Sci.*, **75**, 223-232. https://doi.org/10.1016/j.ijmecsci.2013.07.001.

Shen, H.S. (2007), "Thermal postbuckling behavior of shear deformable FGM plates with temperature-dependent properties", *Int. J Mech. Sci.*, **49**(4), 466-478. https://doi.org/10.1016/j.ijmecsci.2006.09.011.

Talha, M. and Singh, B.N. (2010), "Static response and free vibration analysis of FGM plates using higher order shear deformation theory", *Appl. Math. Model.*, **34**(12), 3991-4011. https://doi.org/10.1016/j.apm.2010.03.034.

Wu, C.P. and Li, H.Y. (2010), "An RMVT-based third-order shear deformation theory of multilayered functionally graded material plates", *Compos. Struct.*, **92**(10), 2591-2605. https://doi.org/10.1016/j.compstruct.2010.01.022.

Yang, J., Liew, K.M. and Kitipornchai, S. (2005), "Stochastic analysis of compositionally graded plates with system randomness under static loading", *Int J Mech. Sci.*, **47**(10), 1519-1541. https://doi.org/10.1016/j.ijmecsci.2005.06.006.

Yiotis, A.J. and Katsikadelis, J.T. (2013), "Analysis of cylindrical shell panels. A meshless solution", *Eng. Anal. Bound. Elem.*, **37**(6), 928-935. https://doi.org/10.1016/j.enganabound.2013.03.005.

Zhang, D.G. and Zhou, Y.H. (2008), "A theoretical analysis of FGM thin plates based on physical neutral surface", *Comput. Mater. Sci.*, **44**, 716-720. https://doi.org/10.1016/j.commatsci.2008.05.016.

Zhang, L.W. and Liew, K.M. (2016), "Element-free geometrically nonlinear analysis of quadrilateral functionally graded material plates with internal column supports", *Compos. Struct.*, **147**, 99-110. https://doi.org/10.1016/j.compstruct.2016.03.034.

CC

Appendix

A.1 Analytical solution of simply supported FG plate

The governing differential equations (11a)-(11c) for the simply supported FG nanoplates can be solved by Navier's approach. According to Navier's approach, the solution can be expressed as:

$$\phi_x = \sum_{m=1}^{\infty}\sum_{n=1}^{\infty} X_{mn}\cos\alpha x\sin\beta y \tag{A1}$$

$$\phi_y = \sum_{m=1}^{\infty}\sum_{n=1}^{\infty} Y_{mn}\sin\alpha x\cos\beta y \tag{A2}$$

$$w = \sum_{m=1}^{\infty}\sum_{n=1}^{\infty} W_{mn}\sin\alpha x\sin\beta y \tag{A3}$$

where X_{mn}, Y_{mn} and W_{mn} are displacement coefficients to be determined, and $\alpha = m\pi/a$ and $\beta = n\pi/b$. While a and b are the length and width of the rectangular FG plates. Moreover, the external load can be written by the Fourier series as:

$$q = \sum_{m=1}^{\infty}\sum_{n=1}^{\infty} Q_{mn}\sin\alpha x\sin\beta y \tag{A4}$$

Substituting Eqs. (A1)-(A3) and (A4) into Eqs. (11a)-(11c) generates a linear system

$$\begin{bmatrix} a_{11} & a_{12} & a_{13} \\ a_{21} & a_{22} & a_{23} \\ a_{31} & a_{32} & a_{33} \end{bmatrix} \begin{Bmatrix} W_{mn} \\ X_{mn} \\ Y_{mn} \end{Bmatrix} = \begin{Bmatrix} Q_{mn} \\ 0 \\ 0 \end{Bmatrix} \tag{A5}$$

where

$$a_{11} = k_s B\left(\alpha^2 + \beta^2\right) \tag{A6}$$

$$a_{12} = k_s B\alpha \tag{A7}$$

$$a_{13} = k_s B\beta \tag{A8}$$

$$a_{21} = k_s B\alpha \tag{A9}$$

$$a_{22} = A\left(\frac{(1-\nu)}{2}\beta^2 + \alpha^2\right) + k_s B \tag{A10}$$

$$a_{23} = A\frac{(1+\nu)}{2}\alpha\beta \tag{A11}$$

$$a_{31} = k_s B\beta \tag{A12}$$

$$a_{32} = A\frac{(1+\nu)}{2}\alpha\beta \tag{A13}$$

$$a_{33} = A\left(\frac{(1-\nu)}{2}\alpha^2 + \beta^2\right) + k_s B \tag{A14}$$

Then, by solving Eq. (A5), the displacement coefficients can be written as:

$$X_{mn} = \frac{(a_{21}a_{33} - a_{23}a_{31})Q_{mn}}{\begin{pmatrix} a_{11}(a_{22}a_{33} - a_{23}a_{32}) \\ +a_{12}(a_{23}a_{31} - a_{21}a_{33}) \\ +a_{13}(a_{21}a_{32} - a_{22}a_{31}) \end{pmatrix}} \tag{A15}$$

$$Y_{mn} = \frac{(a_{21}a_{32} - a_{22}a_{31})Q_{mn}}{\begin{pmatrix} a_{11}(a_{22}a_{33} - a_{23}a_{32}) \\ +a_{12}(a_{23}a_{31} - a_{21}a_{33}) \\ +a_{13}(a_{21}a_{32} - a_{22}a_{31}) \end{pmatrix}} \tag{A16}$$

$$W_{mn} = \frac{(a_{22}a_{33} - a_{23}a_{32})Q_{mn}}{\begin{pmatrix} a_{11}(a_{22}a_{33} - a_{23}a_{32}) \\ +a_{12}(a_{23}a_{31} - a_{21}a_{33}) \\ +a_{13}(a_{21}a_{32} - a_{22}a_{31}) \end{pmatrix}} \tag{A17}$$

Therefore, the solution can be obtained by substituting the displacement coefficients into Eqs. (A1)-(A3).

A.2 The particular solution of $\nabla^2\hat{u}_j = f_j$ and the involved derivatives of $\hat{u}_j$

The particular solution of $\nabla^2\hat{u}_j = f_j$ can be expressed as:

$$\hat{u}_j = \frac{1}{32}r^4(2\ln r - 1) \tag{A18}$$

and by differentiation, it results in

$$\hat{u}_{j,n} = \frac{1}{16}r^3 r_{,n}(4\ln r - 1) \tag{A19}$$

$$\hat{u}_{j,x} = \frac{1}{16}r^3 r_{,x}(4\ln r - 1) \tag{A20}$$

$$\hat{u}_{j,y} = \frac{1}{16}r^3 r_{,y}(4\ln r - 1) \tag{A21}$$

$$\hat{u}_{j,xx} = \frac{1}{16}r^2 r_{,y}^2(4\ln r - 1) + \frac{1}{16}r^2 r_{,x}^2(12\ln r + 1) \tag{A22}$$

$$\hat{u}_{j,yy} = \frac{1}{16} r^2 r_{,x}^2 (4\ln r - 1) + \frac{1}{16} r^2 r_{,y}^2 (12\ln r + 1) \quad \text{(A23)}$$

$$\hat{u}_{j,xy} = \frac{1}{16} r^2 r_{,x} r_{,y} (8\ln r + 2) \quad \text{(A24)}$$

Moreover, it can be readily proved that:

$$\begin{aligned} &\lim_{r\to 0} \hat{u}_j = \lim_{r\to 0} \hat{u}_{j,n} = \lim_{r\to 0} \hat{u}_{j,x} = \lim_{r\to 0} \hat{u}_{j,y} = \\ &\lim_{r\to 0} \hat{u}_{j,xx} = \lim_{r\to 0} \hat{u}_{j,yy} = \lim_{r\to 0} \hat{u}_{j,xy} = 0 \end{aligned} \quad \text{(A25)}$$